Additive Manufacturing 36 (2020) 101502

Contents lists available at ScienceDirect

Additive Manufacturing

journal homepage: www.elsevier.com/locate/addma

The effect of material mixing on interfacial stiffness and strength of multi-material additive manufacturing

Fan Liu[a], Tiantian Li[b], Xihang Jiang[a], Zian Jia[a], Zhiping Xu[c], Lifeng Wang[a,*]

[a] Department of Mechanical Engineering, Stony Brook University, Stony Brook, NY 11794, USA
[b] Engineering Department, University of Cambridge, Trumpington Street, Cambridge, CB2 1PZ, UK
[c] Department of Engineering Mechanics, Tsinghua University, Beijing, 100084, China

ARTICLE INFO

Keywords:
Multi-material additive manufacturing
Material interface
Material jetting
Tensile property
Stiffness
Strength

ABSTRACT

Multi-material additive manufacturing, as an additive manufacturing technique with the ability to simultaneously print multiple materials, is widely used in generating composites with multi-colors, complex multi-material structures, and materials with gradient properties. It also becomes a powerful tool in the study of structure-property relationship in composites, mechanical metamaterials, biological and bioinspired materials. However, the material mixing at the printed interfaces leads to unpredictable material properties which will significantly affect the overall performance of the 3D printed materials or parts. In this study, we systematically investigate the tensile properties, including stiffness and strength, of 3D printed multi-material interfaces. The specimens with double and multiple interfaces are designed, fabricated, and tested. The effect of the material jetting process on the topology of the interface and the effect of printing orientation and material thickness on the mechanical properties are evaluated experimentally. A material mixing model based on hyperbolic tangent function is proposed to quantitatively describe the material property distribution at the interface. The findings reported here provide a deep understanding of the mechanical properties of 3D printed multi-material interfaces, and therefore provide guidelines for the design and fabrication of 3D printed multi-material architectures and materials with desired properties.

1. Introduction

Additive manufacturing, also known as 3D printing, has been rapidly developed during the past several decades [1] to meet different functionality, complexity, and accuracy requirements. With all the advantages of additive manufacturing, multi-material additive manufacturing can print multiple materials simultaneously, which brings added material-specific functionalities and increases the design space [2]. For example, with the multi-material additive manufacturing technique, 3D printed parts can be printed with multiple colors [3]. Fiber-reinforce polymer composites can be printed out with fibers dispersed in a polymer matrix [4]. Gradient metallic structures [5] and metal-ceramic structures [6] are also promising applications of multi-material additive manufacturing. Moreover, multi-material additive manufacturing becomes a powerful tool in the study of structure-property relationships in biological and bioinspired materials [7].

Multi-material jetting techniques, such as PolyJet multi-material printing (PMP), have been widely used in the study of the structure-property relationship of composites, mechanical metamaterials, biological and bioinspired materials. First, it helps to understand the mechanical property of these materials and unravels the underlying mechanisms. For example, with mechanical testing on 3D-printed analogues, the influence of detailed structures on the mechanical properties of biological materials, such as the wavy interfaces in plant seed coats [8], interlocked tablets in nacre [9,10] and osteon structure in bone [11], has been revealed. Second, it is used to guide and optimize the structural design of bioinspired materials. By conducting systematic tests of 3D printed specimens with different geometric parameters, optimized designs with better mechanical properties can be realized [12–18]. Third, it can also be used to validate the optimized designs created by novel design approaches such as multi-material topology optimization [19] and machine learning-based design [20].

In the material jetting printing process, liquid-like base materials are jetted by a heated printhead onto the printing tray and typically cured thermally or through UV light (see Fig. 1). This procedure is repeated for each layer until the final height of the part is reached. For this process, the jetting nozzles in different printheads can jet different materials, including supporting material for overhanging features. Due

* Corresponding author.
E-mail address: lifeng.wang@stonybrook.edu (L. Wang).

https://doi.org/10.1016/j.addma.2020.101502
Received 9 January 2020; Received in revised form 29 May 2020; Accepted 29 July 2020
Available online 05 August 2020

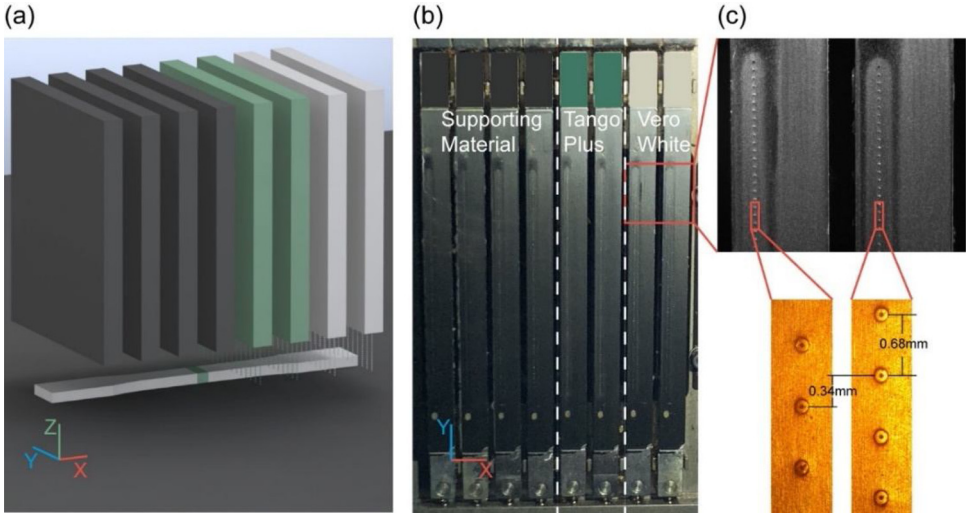

Fig. 1. Printheads of Objet Connex260 3D printer. (a) The schematic of the printing tray and printheads. (b) Eight paralleled printheads allocated to VeroWhite, TangoPlus, and Supporting Material. (c) Jetting nozzles on the printheads.

to the limitation of this technology, the mixing volume between the two materials may affect the properties of the interface. Especially, the mechanical properties of bio-inspired materials with thin material interfaces can be dramatically affected because the property of interfaces is one of the key factors dominating the overall mechanical properties. In several recent studies, it has been found that the mechanical properties predicted from finite element simulations are usually better than those from experimental testing for these multi-material printed specimens [9,21]. Certainly, the differences may attribute to anisotropy, inhomogeneity of jetting materials, and defects between layers during the printing process. In addition, it has been realized the material mixing at the interface of two constituent materials may account for the differences between experiments and simulations [8,22,23]. For example, in the simulation [8], Young's modulus used for the soft interface/material is almost 10 times larger than Young's modulus of pure soft material. Accordingly, to better design and tailor multi-material structures, the interface properties of 3D printed multi-material parts need to be fully investigated.

Recently, extensive research has been conducted on the mechanical properties of 3D printed parts and materials, and many factors are found to be able to significantly affect the results. For example, printing orientation has been proved to influence the mechanical properties especially when the critical load direction is parallel to the vertical direction [24,25]. Other factors, such as finishing process [24], printing speed [26], printing orientation [27], UV exposure time, and material storage time [28] have been well studied. As for the adhesive bonding, the effect of surface roughness on overall strength has been studied and a clear dependency is observed [29,30]. The effect of adhesive thickness has also been investigated both experimentally and numerically [31,32]. Although many researchers have studied the mechanical properties of 3D printed single-material parts and adhesive bonding, however, little is known about the properties of the 3D printed multi-material interfaces. Recently, the mechanical properties on the micron scale [33] have been studied using nanoindentation and showed a smooth transition from stiff material to compliant material. The strength of the interfaces between the constituent 3D printed material and the default mixing materials has also been examined [34]. Moreover, the effects of patterns of graded material interfaces on the fatigue property in material jetted parts have been investigated [35,36]. These findings present a preliminary understanding of the mechanical properties of 3D printed multi-material interfaces.

In this study, we have designed a series of specimens for testing the stiffness and strength at the interface in multi-material additive manufacturing. A Polyjet multi-material 3D printer (Objet Connex260, Stratasys, Ltd) is used to fabricate these specimens. The micro-structures of the interfaces between two 3D printed constituent materials are observed by using an optical microscope. Tensile tests on these 3D printed specimens are conducted, and the effective stiffness and effective strength of specimens with multiple interfaces and different printing orientations are obtained. To quantitatively understand the material mixing and material property transition at multi-material interfaces, a material mixing model based on a two-parameter hyperbolic tangent function is proposed. This material mixing model accurately explains the effect of the printing material thickness and the printing orientation, providing a tool to design complex 3D printed multi-material architectures and composites.

2. Materials and methods

2.1. Sample design

Two groups of dogbone specimens are designed based on TYPE I tensile specimen in ASTM D 638-14 [37]. All specimens are made of two base materials: a rigid polymer material VeroWhite (white part shown in Fig. 2) and one soft rubber-like material TangoPlus (green part shown in Fig. 2). The first group of specimens is designed to obtain the effective strength of the interfaces. One thin layer of TangoPlus is introduced in each VeroWhite specimen, resulting in two interfaces between TangoPlus and VeroWhite, as shown in Fig. 2(a). Specimens with various designed TangoPlus thickness t = 0.1, 0.3, 0.5, 1.0, 2.0, and 6.0 mm are considered to study the thickness effect on the effective strength. In the second group of specimens, multiple TangoPlus thin layers are introduced in each specimen to obtain the effective stiffness of the interfaces, where the thickness of TangoPlus layer varies with t = 0.1, 0.3, 0.5, 1.0, 2.0 and 6.0 mm, but the total TangoPlus thickness in each specimen is kept the same, T = 6.0 mm, leading to the number of TangoPlus layers as $n = T/t$ (see Fig. 2(b)). To study the effect of the printing orientation, these specimens with 5 different printing orientation θ = 0°, 22.5°, 45°, 67.5°, 90° with respect to the printing direction have also been fabricated, as shown in Fig. 2(c). There are 60 designed tensile specimens with different combinations of TangoPlus thickness and printing orientation, and 6 specimens made of pure VeroWhite and TangoPlus for references.

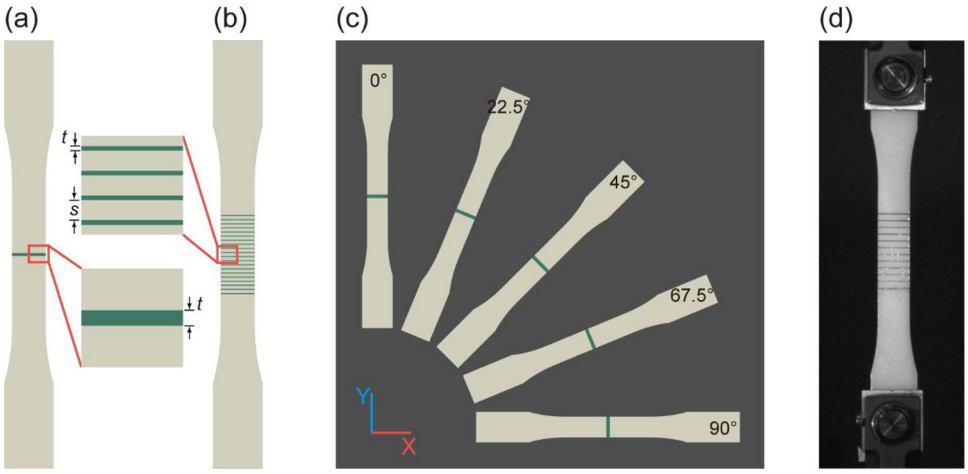

Fig. 2. Specimens for tensile testing. (a) Dogbone samples with a thin layer of TangoPlus/two interfaces for measuring the strength. (b) Dogbone samples with multiple TangoPlus layers but the same total thickness for measuring the stiffness. (c) Designed specimens on the printing tray with 5 printing orientations. (d) A 3D printed specimen loaded on an MTS mechanical tester.

2.2. Sample fabrication

All specimens in this study are fabricated using the Objet Connex260 3D printer (Stratasys, Ltd) which allows printing two different materials simultaneously with PMP technique. The schematic of the printing tray and print heads are shown in Fig. 1(a). The XY plane is the plane of the printing tray and the X-direction is defined as the printing direction. Note that although the printhead moves in both X and Y directions in the PolyJet process, the materials are jetted out from the jetting nozzles only when the printheads move back and forth along the X-direction. Eight printheads are assembled parallel to each other along X-direction. Two printheads are allocated to VeroWhite (marked with white), two to TangoPlus (marked with green), and four to a gel-like supporting material (marked with black). 100 jetting nozzles are equidistantly distributed along Y-direction on each printhead as shown in Fig. 1(b). The distance between two adjacent jetting nozzles on one printhead is 0.68 mm (Fig. 1(c)). For the two printheads allocated to the same material, the distance along Y-direction between two adjacent nozzles on each printhead is 0.34 mm (Fig. 1(c)). In the printing process, the printheads firstly move to a specific position based on the design. Then, the printheads move back and forth along the printing direction (X-direction), meanwhile, the liquid-like base materials are jetted out from the jetting nozzles and cured through UV lights instantly. One layer of the part is generated through such process and the designed part is printed layer by layer until the design height is reached. For all designed samples, 3 identical specimens are fabricated and tested for each data point. All specimens are stored for ~24 h to get fully curing with stable mechanical properties before testing.

2.3. Mechanical testing and optical microscopy observation

Uniaxial tensile tests are performed using an MTS mechanical tester (C43) with 1 kN and 10 kN load cells (Fig. 2(d)). The tensile tests are conducted in a quasi-static regime with a displacement rate of 0.4 mm/min. Digital Image Correlation (DIC) measurement system is used for determining the distance between two designated points within the gage length of the specimen during the test. The load is recorded by the MTS mechanical tester. With the load-displacement curve of the specimen and stiffness value of pure VeroWhite, the stiffness and strength of the soft material with interfaces can be calculated. Note that the load-displacement curves measured from the tests cannot be directly transferred to stress-strain curves because of inhomogeneous deformation, where the total displacement is contributed by two parts: displacement of VeroWhite and displacement of TangoPlus. By removing the displacement of rigid VeroWhite from the total displacement, the stress-strain relation of soft TangoPlus with interfaces can be obtained, and the effective stiffness E_i can, therefore, be calculated as:

$$E_i = \frac{T}{A_0}\frac{f_u - f_l}{(d_u - d_l) - \frac{G-T}{A_0 E_1}(f_u - f_l)} \quad (1)$$

where, $(d_u, f_u)$and $(d_l, f_l)$are the upper and lower points of the linear region of the measured load-displacement curve. A_0 is the original cross-sectional area, $A_0 = 65\text{mm}^2$. G is the gage length, $G = 50\text{mm}$. E_1 is the modulus of the pure VeroWhite. The effective strength of σ_u is defined as $\sigma_u = W/A_0$, where W is the maximum load. The interfaces are examined under an AmScope optical microscope equipped with an Amscope MU1000 microscope digital camera. The color and texture of the two materials are observed. The light source is adjusted carefully to obtain pictures with high contrast between two materials. Two objectives of 4X and 10X are used for the overall and detailed structure of the interfaces. Moreover, the microscope is calibrated with a calibration slide to measure the dimension.

3. Results and discussion

3.1. Micro-structures of the interfaces

Specimens with TangoPlus thickness $t = 0.1$ mm, 0.3 mm, 1.0 mm, and printing orientation $\theta = 0^\circ, 45^\circ, 90^\circ$ are imaged as shown in Fig. 3(a–c). White dashed lines mark represents the designed boundaries of the interface, the printing directions are the X-directions shown in the figures. For specimens with $t = 0.3$ mm, 1.0 mm, a clear interface between TangoPlus and VeroWhite can be observed since the light transmittance of TangoPlus is much higher than that of VeroWhite. However, for specimens with $t = 0.1$ mm, the interface boundaries are not clearly shown in the image. These two materials are mixed together at the interface. Comparing the interfaces with different printing orientations in Fig. 3(b) and (c), interfaces with printing orientation $\theta = 0^\circ$ show clear boundaries, and the actual thicknesses of TangoPlus are nearly the same as the designed thickness. Interfaces with printing orientation $\theta = 45^\circ, 90^\circ$ have fuzzy boundaries and the actual thicknesses of TangoPlus are slightly smaller than the designed thickness. Apparently, printing orientations do affect the micro-structures of the interfaces. Fig. 3(d) shows clear straight boundary line at the interface with printing orientation $\theta = 0^\circ$, while drop-shaped structures are found at interfaces with printing orientation $\theta = 45^\circ, 90^\circ$, and the directions of the drop-shaped structures are the same as the corresponding printing orientations. The distance between two droplets is ~0.34 mm, which is identical to the distance between two jetting nozzles as mentioned previously. Moreover, under the layer of drop-shaped structures on the surface, another layer of drop-shaped structures can be observed at the interface with printing orientation $\theta = 90^\circ$. All these indicate that the drop-shaped structures formed from the material jetting process at different printing orientations will affect the

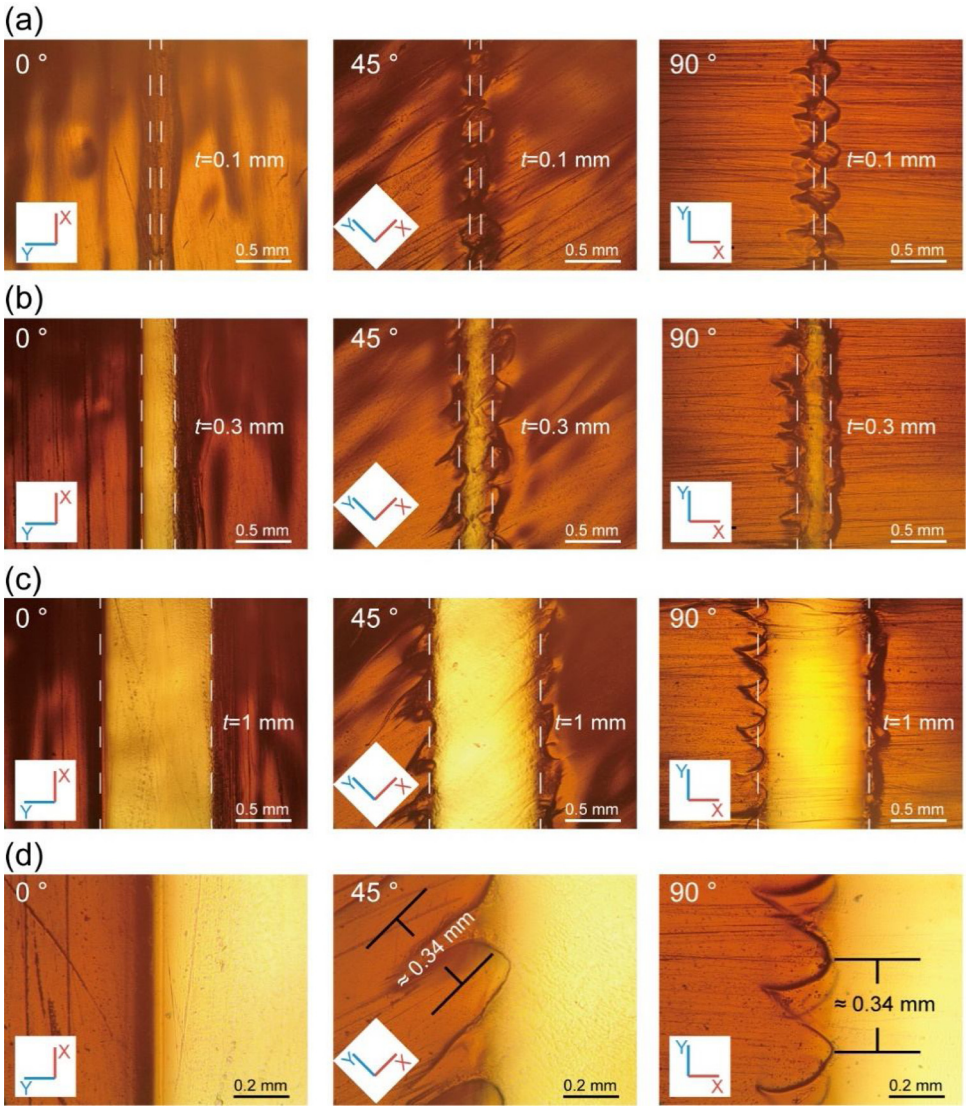

Fig. 3. Micro-structures of the interfaces. (a-c) Microphotographs of interfaces with TangoPlus thickness $t = 0.1$ mm, 0.3 mm, 1.0 mm and printing orientation $\theta = 0^{\circ}$, 45°, 90°. (d) Microphotographs of boundaries of interfaces with printing orientation $\theta = 0^{\circ}$, 45°, 90°.

material mixing at the interface and further the mechanical properties.

3.2. Mechanical response under tensile loading

Fig. 4 shows the typical load-displacement curves of specimens with $t = 0.1$ mm, 1.0 mm, 6.0 mm and $\theta = 0^{\circ}$, 45°, 90° under tensile loading. Interestingly, fractures always occur in TangoPlus even though some of them are very close to the interfaces. The interfacial adhesion between two materials formed upon printing is strong so that the specimens do not fail at the interface region. This is consistent with previous studies [34,38], in which most of the specimens did not fail at the interfaces. Although a few specimens were "observed" to have interface failure in their studies, however, the location of the fractures was not exactly on the interface because clear same residual materials can be observed on both sides of the broken specimens. For the cases of $t = 0.1$ mm, a sudden drop is observed at small displacement, indicating catastrophic failures that are evidenced in the deformation images before and after the sudden drops (Fig. 4(a)). The cracks initiate and propagate through TangoPlus and the fracture surfaces are very smooth. Because the thickness of TangoPlus is small, the total failure displacement is small. However, for the case of $t = 1.0$ mm, as shown in Fig. 4(b), there are 2 peaks in the load-displacement curves and the load gradually drops to 0 after the second peak. The first peak indicates the yielding of interface materials, however, which are not simple rubber. After that, multiple voids appear in the designed TangoPlus area before complete failure, leading to rough fracture surfaces after failure. The second peak corresponds to the progressive failure of all ligaments formed between voids. Clearly, the material mixing and the resulting inhomogeneous stress distribution are playing a significant role to cause this failure mode. For the cases of $t = 6.0$ mm, a sudden drop is observed at a much larger displacement, and the images show a typical failure behavior of rubber with a flat and smooth fracture surface. As for the effect of printing orientation θ, similar load-displacement curves and fracture surfaces are observed with different printing orientations, which implies that printing orientation θ can hardly affect the failure modes in this study.

Fig. 4(d) shows the DIC measurement result of strain distributions of specimens with single and multiple layers of TangoPlus with $t = 2.0$ mm. It demonstrates the stiffer material has much lower strain while the softer material has higher strain as expected. Near the interface, a clear graded strain transition region is observed, indicating that material mixing occurs in that region, which will be modeled quantitatively in the next section. Generally, the strain distribution in each material is homogeneous under such uniaxial loading condition.

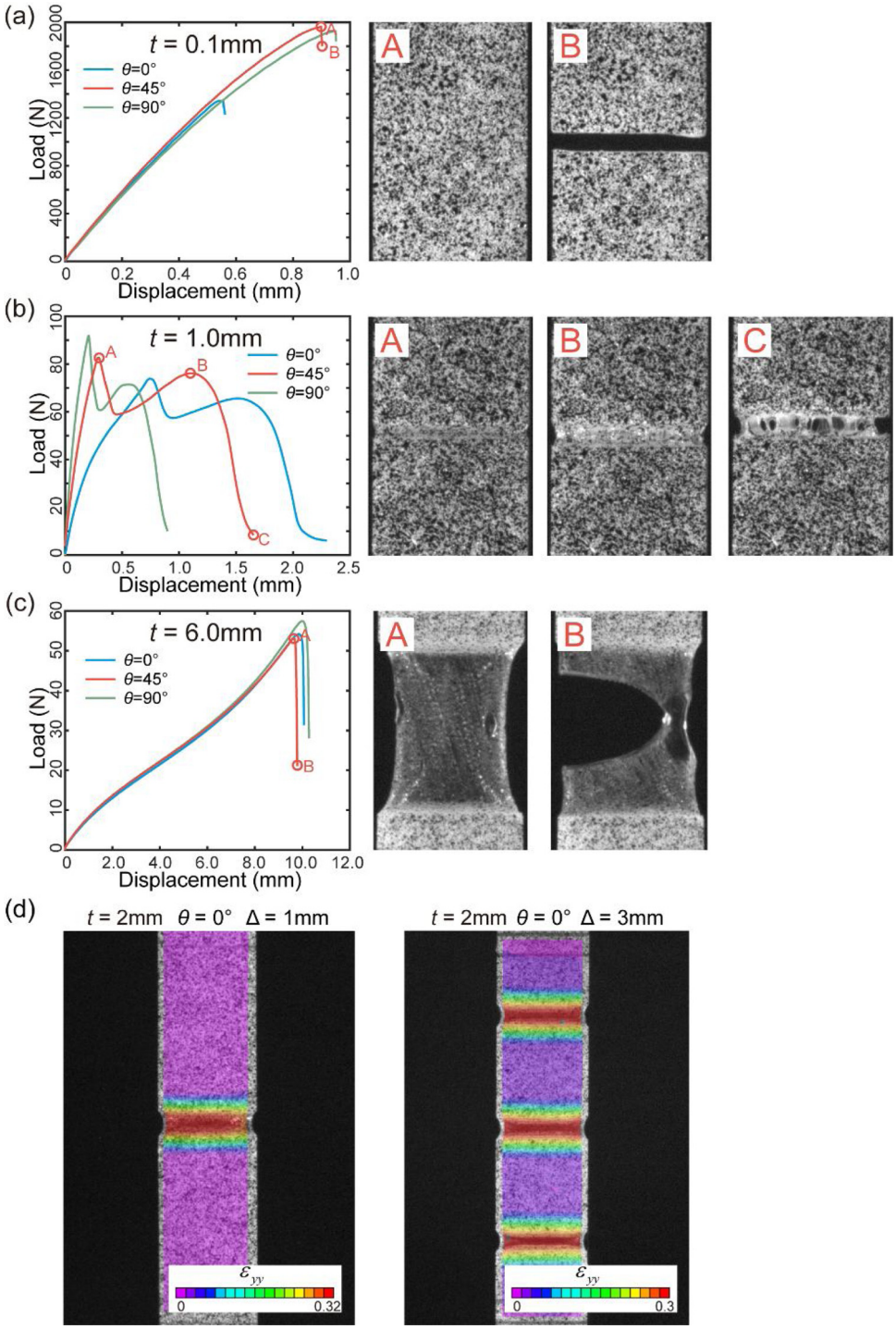

Fig. 4. Typical load-displacement curves, deformation and strain distributions. (a) $t = 0.1$ mm. (b) $t = 1.0$ mm. (c) $t = 6.0$ mm. (d) DIC strain distributions of specimens with single and multiple thin layers of TangoPlus, $t = 2.0$ mm.

Fig. 5 shows experimental results of the effective stiffness and effective strength of TangoPlus with interfaces with t = 0.1, 0.3, 0.5, 1.0, 2.0, and 6.0 mm, calculated from the load-displacement curves. The stiffness and strength of VeroWhite (2192 MPa and 40.4 MPa) and TangoPlus (0.486 MPa and 0.421 MPa) are also shown for comparison. In general, the results have a good consistency. All the effective stiffness and effective strength increase with the decrease of TangoPlus thickness dramatically, showing a strong interface effect. The effective stiffness can vary from 0.6 MPa ($t = 6.0$ mm) to more than 400 MPa ($t = 0.1$ mm), while the effective strength varies from 0.8 MPa ($t = 6.0$ mm) to more than 20 MPa ($t = 0.1$ mm). This also indicates the thickness of the material mixing area is comparable to the designed TangoPlus thickness of 0.1 mm so that the material properties are significantly differentiated from TangoPlus. Note that in the tests for the effective strength, in each specimen the number of interfaces is fixed as 2, but the number of interfaces is up to 120 in the tests for the effective stiffness. The quantitative discussions will be provided in the next section.

Printing orientation can also affect the tensile properties. It is possible to see a trend that the effective stiffness and effective strength increase $\sim 2-3$ times when printing orientation changing from 0° to 90° with smaller TangoPlus thickness. However, when the thickness is larger, $t = 6.0$ mm, the printing orientation has no clear influence on the

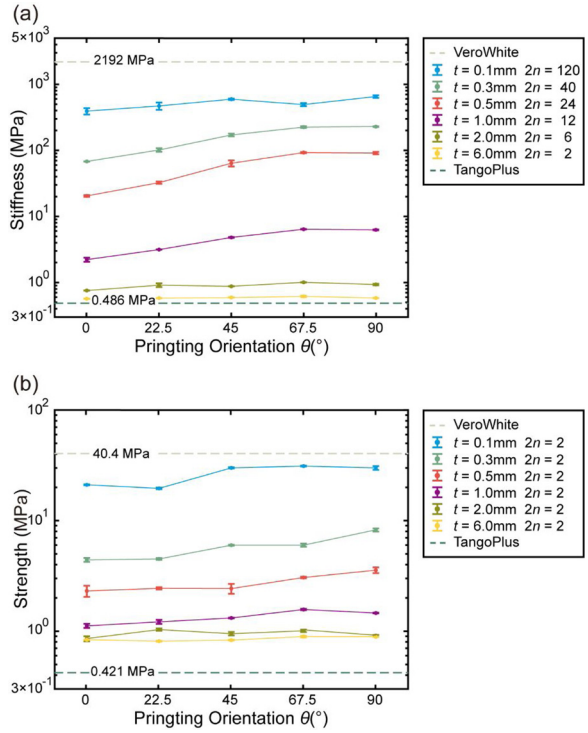

Fig. 5. Calculated effective tensile properties of TangoPlus with the corresponding interfaces from experiments. (a) Effective stiffness. (b) Effective strength. In each specimen, the designed thickness of TangoPlus t = 0.1–6.0 mm and the number of interfaces $2n$ = 2–120.

tensile properties. To further study the effect of printing orientation on the effective stiffness and effective strength, a coefficient of variation (CV) has been calculated quantitatively:

$$CV = \frac{\sqrt{\frac{\sum(E_i - \overline{E})^2}{5}}}{\overline{E}} \tag{2}$$

where E_i is the effective stiffness; i from 1 to 5, indicate 5 different printing orientation; $\overline{E}$ is the average value of the effective stiffness. CV of the effective stiffness and effective strength for each group of TangoPlus thickness and 2 base materials (VeroWhite and TangoPlus) are shown in Fig. 6. In general, the effect of printing orientation on the effective stiffness is greater than the effect on the effective strength. For the base materials, the CVs of stiffness and strength are all very small (less than 3 %), which indicates the printing orientation has a small influence on the mechanical properties of pure material printing. The CVs have the largest values when t = 0.3 mm and 0.5 mm, and decrease with the increase of TangoPlus thickness. When t is larger than 2.0 mm, the CVs of both effective stiffness and effective strength is less than 10 %. These results indicate that the printing orientation can affect the micro-structures of the interfaces, and further affect the mechanical responses of the specimens under tensile tests. Especially, when the TangoPlus thickness is smaller and close to 2 times the thickness of the material mixing area, the effect is more significant.

3.3. Material mixing model

To quantitatively explain the difference of the tensile properties caused by different material thicknesses and printing orientations, the thickness of the mixing area, and the properties transition in the mixing area need to be further studied. Note that the material mixing range is very narrow, ~0.2 mm at each interface (Fig. 3(d)), however, it cannot explain the stiffness discrepancy observed with t = 2.0 mm and t = 6.0 mm. During the printing process, a roller moves back and forth to smooth out the jetted material and prepare a flat surface for the next layer. The material mixing range could be expanded, which can be hard to observe directly (still we can find traces in Fig. 3(c)), but dramatically change the mechanical properties. To describe the material mixing area and the material property transition in the mixing area, a sound material mixing model is needed.

Different forms of hyperbolic tangent functions have been used to describe the variations of material properties of functionally graded material and polymers at different temperatures [39,40]. While graded distribution has also been observed in the mixing areas, a hyperbolic tangent function is assumed to describe the mechanical properties transition. The designed boundary of the interface is marked with a red dashed line in Fig. 7(a). In theory, the material on the left side of the designed boundary is VeroWhite while TangoPlus on the right side. Due to the material mixing, there is a mixing area near the designed boundary where the material property is generally changed from VeroWhite to TangoPlus as shown in Fig. 7(a). The printing orientation affects the position and the thickness of the mixing area, where the effective material stiffness distribution can be described by 2 parameters a and b in the hyperbolic tangent function:

$$E(x) = \frac{1}{2}(E_1 + E_2) + \frac{1}{2}(E_1 - E_2)\tanh\left(\frac{(x+b)}{a}\right) \tag{3}$$

where $E(x)$ is Young's modulus distribution in the mixing area. E_1 and E_2 are Young's modulus of VeroWhite and TangoPlus, respectively. a is a parameter proportional to the thickness of the material mixing area. For the perfectly designed case, a = 0. b represents the shift of the inflection point in the hyperbolic tangent function as shown in Fig. 7(a). Therefore, the equivalent stiffness distribution at the interface as a function of t and θ can be obtained as:

$$E(t,\theta) = \frac{t}{2}\cdot\frac{E_1}{E_1\cdot\int_{-\frac{1}{2}s}^{\frac{1}{2}t}\frac{e^{\frac{2}{a(\theta)}(x+b(\theta))}+1}{E_2\cdot e^{\frac{2}{a(\theta)}(x+b(\theta))}+E_1}dx - s} \tag{4}$$

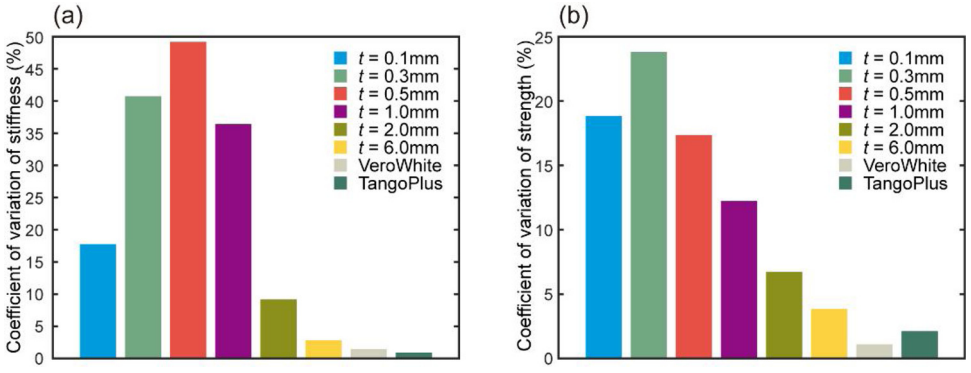

Fig. 6. (a) Coefficient of variation of the effective stiffness. (b) Coefficient of variation of the effective strength.

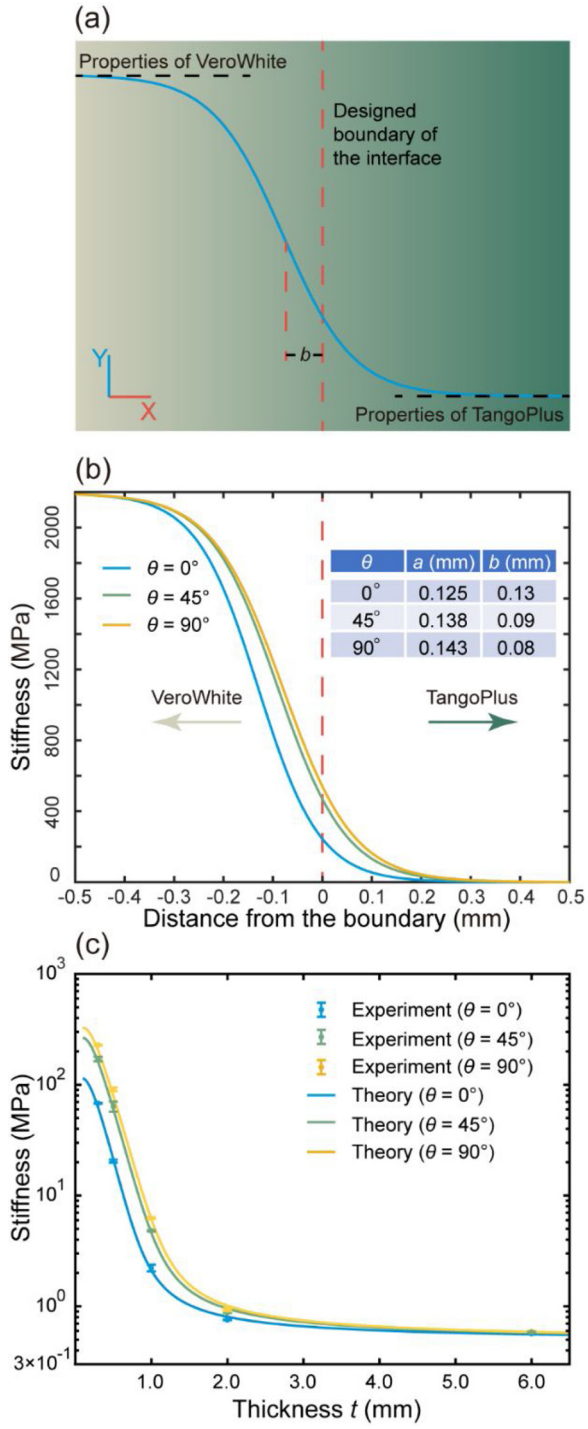

Fig. 7. Material mixing model based on hyperbolic tangent function. (a) Schematic material mixing area and material property transition curve based on hyperbolic tangent function. (b) Material property transition curves of interfaces with different printing orientation. (c) Theoretical and experimental results of the effective stiffness as a function of the designed TangoPlus thickness.

where s is the designed distance between two interfaces (see Fig. 2(b)). The fitting values of a and b and the corresponding hyperbolic tangent functions of stiffness for interface with printing orientation $\theta = 0^{\circ}$, 45°, 90° are shown in Fig. 7(b). a increases from 0.125 mm to 0.143 mm when θ changes from 0° to 90°, explaining why the effective stiffness with $\theta = 90^{\circ}$ has higher values. Based on the material mixing model and the calculated parameters a and b, theoretical predictions of the effective stiffness as a function of designed TangoPlus thickness have been calculated, as shown in Fig. 7(c). The theoretical results and experimental values match well, which implies the material mixing model can accurately describe the effect of printing orientation and material thickness on the measure of effective stiffness.

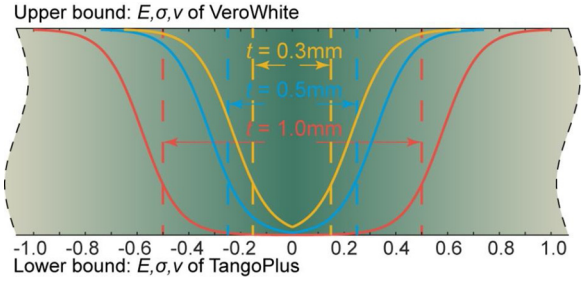

Fig. 8. Material property distributions at the interfaces with t = 0.3, 0.5 and 1.0 mm.

Fig. 8 shows the material property distributions at the interfaces of three designed TangoPlus thicknesses based on the material mixing model, where the material property of VeroWhite is the upper bound and that of TangoPlus is the lower bound. When the designed thickness is smaller than 0.3 mm, the material property of the designed TangoPlus region is clearly different from the pure TangoPlus. This is consistent with previous studies [8]. However, when the designed TangoPlus thickness is larger than 1.0 mm, the material properties between 2 interfaces can reach the lower bound as pure TangoPlus. Fig. 8 clearly explains the effective tensile properties observed in Fig. 5 where the designed thickness of TangoPlus has a significant effect. The effective stiffness relies on the number of interfaces, but the effective strength depends more on the thickness of each TangoPlus layer.

Regarding the effective strength, it's hard to determine where the material yields first based on Fig. 8 because of highly inhomogeneous material distribution in the specimens (not necessary at the center of TangoPlus, such as the region close to the edge). A finite element model is developed for the further study of the effective strength observed in Fig. 5. As shown in Fig. 9(a), a ¼ model is created due to the symmetric boundary conditions. In the mixing area, the mesh size is as small as 0.01 mm. Based on the position of each element, the material properties are assigned accordingly from the material mixing model (Fig. 8), where E, σ, and v that used in FE simulation are calculated using Eq. (4), correspondingly. The same parameters a and b are used for all E, σ, and v although they are determined from the modulus data only. Despite the microstructures observed in Fig. 3, it is assumed that the material property transition is smooth and uniform. Fig. 9(b) show the simulation results of the effective strength as a function of designed TangoPlus thickness for $\theta = 0^{\circ}$, 45°, and 90°. It is consistent with the experimental results that the effective strength increases with the decrease of TangoPlus thickness. However, experimental values are clearly smaller than the FEM predictions when TangoPlus thickness is small. This is due to the uncertainties at the interface area in the specimens, including the microstructures observed previously, the defects introduced during the 3D printing process, and the inhomogeneity in the material mixing. Another reason could be that the strength data defined for each element in the FE simulation are not sufficiently accurate. Because the stress and strain distributions in TangoPlus and the interfaces are largely not homogeneous and not changing uniformly, the introduction of errors is unavoidable. To obtain a more accurate prediction, a more sophisticated model needs to be developed, which is not covered in the current paper.

4. Conclusion

The interface properties are of critical importance to the overall performance of multifunctional structures and composites fabricated by multi-material additive manufacturing. This paper systematically

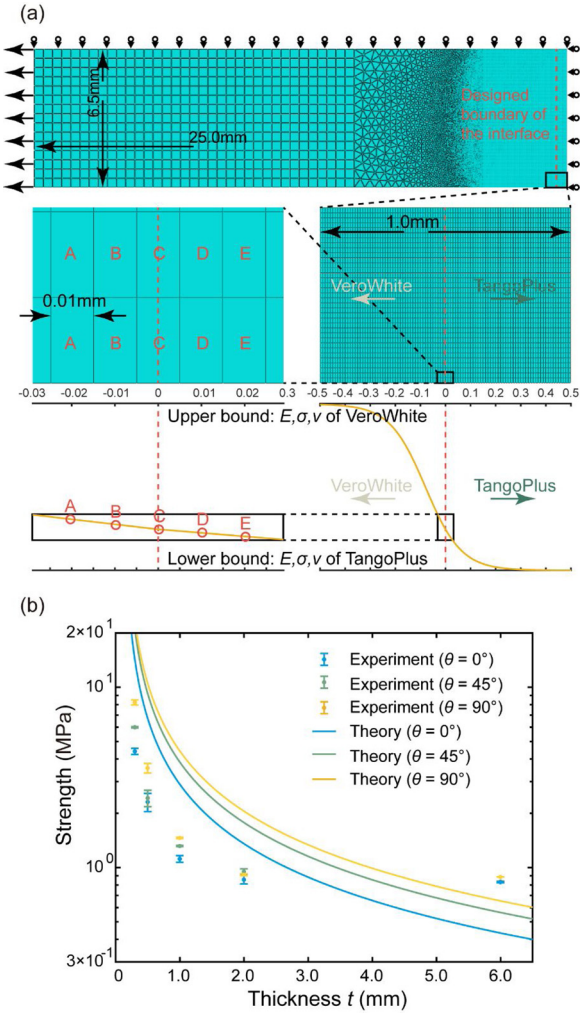

Fig. 9. FEM simulation based on the material mixing model. (a) FEM model and material distribution based on the hyperbolic tangent function. (b) Simulation and experimental results of the effective strength.

investigates the tensile properties of multi-material interfaces fabricated via PolyJet multi-material printing technique. The effective stiffness and strength are found to be strongly dependent on the interfacial material thickness and the printing orientation. Interfaces between rigid and compliant materials are found to be strong due to the material mixing during the printing process, where the material property distribution can be quantitatively described. It is suggested that the minimum thickness of the printed material in the multi-material jetting should be larger than $2a$ (~0.28 mm in current study) in order to minimize the interface effects. The material mixing model developed in this study successfully predicts the effective stiffness and effective strength calculated from the experiments. The findings here present an important understanding of the microstructural mechanics and properties of 3D printed multi-material parts and materials, where the interfacial behavior plays an important role.

CRediT authorship contribution statement

Fan Liu: Conceptualization, Methodology, Investigation, Formal analysis, Visualization, Writing - original draft. **Tiantian Li:** Methodology, Investigation, Formal analysis. **Xihang Jiang:** Methodology, Investigation, Formal analysis. **Zian Jia:** Methodology, Investigation, Formal analysis. **Zhiping Xu:** Conceptualization, Investigation, Writing - review & editing. **Lifeng Wang:** Conceptualization, Methodology, Investigation, Supervision, Validation, Writing - review & editing.

Declaration of Competing Interest

The authors declare that they have no known competing financial interests or personal relationships that could have appeared to influence the work reported in this paper.

Acknowledgment

This research was partly supported by the National Science Foundation (CMMI-1462270). The authors acknowledge the use of the Center for Functional Nanomaterials facility at Brookhaven National Laboratory.

References

[1] T.D. Ngo, A. Kashani, G. Imbalzano, K.T. Nguyen, D. Hui, Additive manufacturing (3D printing): a review of materials, methods, applications and challenges, Compos. Part B: Eng. 143 (2018) 172–196.
[2] A. Bandyopadhyay, B. Heer, Additive manufacturing of multi-material structures, Mater. Sci. Eng. R Rep. 129 (2018) 1–16.
[3] K.-J. Chang, Color or multi-material three-dimensional (3D) printing, US Patent: US9688022B2, 2017.
[4] C.C. Spackman, C.R. Frank, K.C. Picha, J. Samuel, 3D printing of fiber-reinforced soft composites: process study and material characterization, J. Manuf. Process. 23 (2016) 296–305.
[5] D.C. Hofmann, J. Kolodziejska, S. Roberts, R. Otis, R.P. Dillon, J.-O. Suh, Z.-K. Liu, J.-P. Borgonia, Compositionally graded metals: a new frontier of additive manufacturing, J. Mater. Res. 29 (17) (2014) 1899–1910.
[6] T. Gualtieri, A. Bandyopadhyay, Additive manufacturing of compositionally gradient metal-ceramic structures: stainless steel to vanadium carbide, Mater. Des. 139 (2018) 419–428.
[7] A. Velasco-Hogan, J. Xu, M.A. Meyers, Additive manufacturing as a method to design and optimize bioinspired structures, Adv. Mater. 30 (52) (2018) 1800940.
[8] C. Gao, B.P. Hasseldine, L. Li, J.C. Weaver, Y. Li, Amplifying strength, toughness, and auxeticity via wavy sutural tessellation in plant seedcoats, Adv. Mater. 30 (36) (2018) 1800579.
[9] S. Askarinejad, H.A. Choshali, C. Flavin, N. Rahbar, Effects of tablet waviness on the mechanical response of architected multilayered materials: modeling and experiment, Compos. Struct. 195 (2018) 118–125.
[10] F. Liu, T. Li, Z. Jia, L. Wang, Combination of stiffness, strength, and toughness in 3D printed interlocking nacre-like composites, Extreme Mech. Lett. 35 (2020) 100621.
[11] Z. Jia, L.F. Wang, 3D printing of biomimetic composites with improved fracture toughness, Acta Mater. 173 (2019) 61–73.
[12] E. Lin, Y. Li, J.C. Weaver, C. Ortiz, M.C. Boyce, Tunability and enhancement of mechanical behavior with additively manufactured bio-inspired hierarchical suture interfaces, J. Mater. Res. 29 (17) (2014) 1867–1875.
[13] L. Wang, J. Lau, E.L. Thomas, M.C. Boyce, Co-continuous composite materials for stiffness, strength, and energy dissipation, Adv Mater 23 (13) (2011) 1524–1529.
[14] Z. Jia, Y. Yu, L.F. Wang, Learning from nature: use material architecture to break the performance tradeoffs, Mater Design 168 (2019) 107650.
[15] Z.A. Jia, T.T. Li, F.P. Chiang, L.F. Wang, An experimental investigation of the temperature effect on the mechanics of carbon fiber reinforced polymer composites, Compos. Sci. Technol. 154 (2018) 53–63.
[16] T.T. Li, Y.Y. Chen, X.Y. Hu, Y.B. Li, L.F. Wang, Exploiting negative Poisson's ratio to design 3D-printed composites with enhanced mechanical properties, Mater Design 142 (2018) 247–258.
[17] T.T. Li, Y.Y. Chen, L.F. Wang, Enhanced fracture toughness-in architected-interpenetrating phase composites by 3D printing, Compos. Sci. Technol. 167 (2018) 251–259.
[18] P. Zhang, M.A. Heyne, A.C. To, Biomimetic staggered composites with highly enhanced energy dissipation: modeling, 3D printing, and testing, J. Mech. Phys. Solids 83 (2015) 285–300.
[19] P. Vogiatzis, S. Chen, X. Wang, T. Li, L. Wang, Topology optimization of multi-material negative Poisson's ratio metamaterials using a reconciled level set method, J. Technol. Comput. Aided Des. Tcad 83 (2017) 15–32.
[20] G.X. Gu, C.-T. Chen, D.J. Richmond, M.J. Buehler, Bioinspired hierarchical composite design using machine learning: simulation, additive manufacturing, and experiment, Mater. Horiz. 5 (5) (2018) 939–945.
[21] J.H. Epstein, S.J. Anthony, A. Islam, A.M. Kilpatrick, S.A. Khan, N. Ross, I. Smith, J. Barr, C. Zambrana-Torrelio, Y. Tao, A. Islam, P.L. Quan, K. Olival, E. Gurley, M.J. Hossain, H.E. Field, M. Fielder, T. Briese, M. Rahman, G. Crameri, L.F. Wang, S. Luby, W.I. Lipkin, P. Daszak, Nipah virus ecology and infection dynamics in its bat reservoir, Pteropus medius, in Bangladesh, Int. J. Infect. Dis. 53 (2016) 20–21.
[22] L.S. Dimas, G.H. Bratzel, I. Eylon, M.J. Buehler, Tough composites inspired by mineralized natural materials: computation, 3D printing, and testing, Adv. Funct. Mater. 23 (36) (2013) 4629–4638.
[23] I. Vu, L. Bass, N. Meisel, B. Orler, C.B. Williams, D.A. Dillard, Characterization of mutli-material interfaces in PolyJet additive manufacturing, Solid Freeform Fabr.

Symp. Proc. (2014) 959–982.
[24] A. Cazón, P. Morer, L. Matey, PolyJet technology for product prototyping: tensile strength and surface roughness properties, Proc. Inst. Mech. Eng. Part B: J. Eng. Manuf. 228 (12) (2014) 1664–1675.
[25] P. Gay, D. Blanco, F. Pelayo, A. Noriega, P. Fernández, Analysis of factors influencing the mechanical properties of flat PolyJet manufactured parts, Procedia Eng. 132 (2015) 70–77.
[26] A. Pilipović, P. Raos, M. Šercer, Experimental analysis of properties of materials for rapid prototyping, Int. J. Adv. Manuf. Technol. 40 (1–2) (2009) 105–115.
[27] I.Q. Vu, L.B. Bass, C.B. Williams, D.A.J.A.M. Dillard, Characterizing the effect of print orientation on interface integrity of multi-material jetting additive manufacturing, Addit. Manuf. 22 (2018) 447–461.
[28] J. Mueller, S. En Kim, K. Shea, C. Daraio, Tensile properties of inkjet 3D printed parts: critical process parameters and their efficient analysis, The American Society of Mechanical Engineers, 35th Computers and Information in Engineering Conference, Vol. 1A 2015 pp. DETC2015-4802.
[29] T. Brosh, R. Pilo, N. Bichacho, R. Blutstein, Effect of combinations of surface treatments and bonding agents on the bond strength of repaired composites, J. Prosthet. Dent. 77 (2) (1997) 122–126.
[30] S. Budhe, A. Ghumatkar, N. Birajdar, M. Banea, Effect of surface roughness using different adherend materials on the adhesive bond strength, Appl. Adhes. Sci. 3 (1) (2015) 20.
[31] L.F. Da Silva, T. Rodrigues, M. Figueiredo, M. De Moura, J. Chousal, Effect of adhesive type and thickness on the lap shear strength, J. Adhes. 82 (11) (2006) 1091–1115.
[32] W. Xu, Y. Wei, Influence of adhesive thickness on local interface fracture and overall strength of metallic adhesive bonding structures, Int. J. Adhes. Adhes. 40 (2013) 158–167.
[33] J. Mueller, D. Courty, M. Spielhofer, R. Spolenak, K. Shea, Mechanical properties of interfaces in inkjet 3D printed single-and multi-material parts, 3D Print. Addit. Manuf. 4 (4) (2017) 193–199.
[34] T.S. Lumpe, J. Mueller, K. Shea, Tensile properties of multi-material interfaces in 3D printed parts, Mater. Des. 162 (2019) 1–9.
[35] D.V. Kaweesa, N.A. Meisel, Quantifying fatigue property changes in material jetted parts due to functionally graded material interface design, Addit. Manuf. 21 (2018) 141–149.
[36] D.V. Kaweesa, D.R. Spillane, N.A. Meisel, Investigating the impact of functionally graded materials on fatigue life of material jetted specimens, Solid Freeform Fabr. Symp. Proc. (2017) 578–592.
[37] A. International, A.S.T.M. D638-14, Standard test method for tensile properties of plastics, ASTM International (2015).
[38] J.P. Moore, C.B. Williams, Fatigue characterization of 3D printed elastomer material, Int. Solid Freeform Fabr. Symp. (2012) 641–655.
[39] S.-H. Chi, Y.-L. Chung, Mechanical behavior of functionally graded material plates under transverse load—part I: analysis, Int. J. Solids Struct. 43 (13) (2006) 3657–3674.
[40] B.L. Volk, D.C. Lagoudas, Y.-C. Chen, Analysis of the finite deformation response of shape memory polymers: II. 1D calibration and numerical implementation of a finite deformation, thermoelastic model, Smart Mater. Struct. 19 (7) (2010) 075006.